observations that the anisotropy is weakest at the youngest ages (where melt content should be highest) and does not decay with age as the lithosphere cools are both inconsistent with this scenario. I conclude that the most likely explanation for the anomalous anisotropy is lithospheric fabric formed during hotspot-fueled buoyant upwelling at the RR.

This result has a number of implications for the dynamics of hotspot-ridge systems. It provides unique observational evidence that buoyancy-driven upwelling is an important component of ridge dynamics, especially in environments where passive sea-floor spreading is too slow to accommodate melt production. The presence of anomalous mantle fabric to a depth of ~100 km implies that the hotspot modulates upper-mantle dynamics beneath the ridge to at least this depth. Although I cannot directly estimate the temperature of the hotspot source, the 30- to 80-K anomaly inferred for the RR provides a constraint on temperature in numerical models of plume-ridge interaction. Finally, this result implies that the anisotropic structure of oceanic lithosphere may not be as simple as inferred through studies from the fast-spreading Pacific ridges, and that this structure holds important clues to ridge and plume dynamics.

References and Notes

1. C. J. Wolfe, I. T. Bjarnason, J. C. VanDecar, S. C. Solomon, *Nature* **385**, 245 (1997).
2. G. R. Foulger *et al.*, *Geophys. J. Int.* **142**, 1 (2000).
3. P. R. Vogt, *Earth Planet. Sci. Lett.* **13**, 153 (1971).
4. R. C. Searle *et al.*, *Earth Planet. Sci. Lett.* **160**, 463 (1998).
5. J. R. Smallwood, R. S. White, *J. Geophys. Res.* **203**, 5185 (1998).
6. J.-G. Schilling, *Nature* **242**, 565 (1973).
7. J. G. Fitton, A. D. Saunders, M. J. Norry, B. Hardarson, R. N. Taylor, *Earth Planet. Sci. Lett.* **153**, 197 (1997).
8. M. M. Yale, J. Phipps Morgan, *Earth Planet. Sci. Lett.* **161**, 45 (1998).
9. G. Ito, Y. Shen, G. Hirth, C. J. Wolfe, *Earth Planet. Sci. Lett.* **165**, 81 (1999).
10. G. Ito, *Nature* **411**, 681 (2001).
11. R. E. Bell, W. R. Buck, *Nature* **357**, 583 (1992).
12. Earthquake source parameters were obtained from Harvard University's Centroid Moment Tensor (CMT) catalog (www.seismology.harvard.edu).
13. J.-P. Montagner, T. Tanimoto, *J. Geophys. Res.* **96**, 20337 (1991).
14. G. Ekström, A. M. Dziewonski, *Nature* **394**, 168 (1998).
15. J. Ritsema, H. J. van Heijst, J. H. Woodhouse, *Science* **286**, 1925 (1999).
16. Synthetics were calculated via mode summation and were complete to 50 mHz, and perturbation theory was applied to correct each synthetic for the mean along-path bathymetry.
17. A. Nicolas, N. I. Christensen, in *Composition, Structure, and Dynamics of Lithosphere-Asthenosphere System*, K. Fuchs, C. Froidevaux, Eds., vol. 16 of *Geodynamics Series* (American Geophysical Union, Washington, DC, 1987), pp. 111–123.
18. N. M. Ribe, *J. Geophys. Res.* **97**, 8737 (1992).
19. S. Zhang, S.-I. Karato, *Nature* **375**, 774 (1995).
20. C. E. Nishimura, D. W. Forsyth, *Geophys. J.* **96**, 203 (1989).
21. J. J. Leveque, E. Debayle, V. Maupin, *Geophys. J. Int.* **133**, 529 (1998).
22. J. B. Gaherty, T. H. Jordan, L. S. Gee, *J. Geophys. Res.* **101**, 22291 (1996).
23. L. S. Gee, T. H. Jordan, *Geophys. J. Int.* **111**, 363 (1992).
24. This procedure calculates frequency-dependent phase delays and associated Frechet derivatives. It involves the cross-correlation of data and complete synthetics with a synthetic seismogram constructed for a target wave group, in this case fundamental mode surface waves. The method allows for consistent measurement and interpretation of phase delays, even in the case where substantial higher-mode energy is present.
25. Radial anisotropy is defined by five elastic parameters: the speeds of horizontally and vertically propagating *P* waves, $v_{PH}(z)$ and $v_{PV}(z)$; the speed of horizontally propagating, transversely polarized shear waves, $v_{SH}(z)$; the speed of a shear wave propagating horizontally with a vertical polarization or vertically with horizontal polarization, $v_{SV}(z)$; and a parameter that governs speeds at oblique propagation angles, $\eta(z)$. A complete description of the azimuthal anisotropy requires eight additional parameters [e.g., (*13*)], but we cannot resolve these terms because our data span a narrow azimuth range. Although there are tradeoffs between the radial and azimuthal terms that may bias the anisotropy estimate, the depth distribution is generally robust [e.g., (*34*)].
26. R. S. White, *Philos. Trans. R. Soc. London Ser. A* **355**, 319 (1997).
27. Olivine fabric with a predominantly horizontal orientation cannot preferentially enhance Rayleigh speeds because horizontally polarized Love waves are always relatively fast as well in such a medium (*34*).
28. H.-C. Nataf, I. Nakanishi, D. L. Anderson, *J. Geophys. Res.* **91**, 7261 (1986).
29. S. Webb, D. W. Forsyth, *Science* **280**, 1227 (1998).
30. C. J. Wolfe, S. C. Solomon, *Science* **280**, 1230 (1998).
31. D. K. Blackman *et al.*, *Geophys. J. Int.* **127**, 415 (1996).
32. G. Silveira, E. Stutzmann, D.-A. Griot, J.-P. Montagner, L. Mendes Victor, *Phys. Earth Planet. Inter.* **106**, 257 (1998).
33. K. Barnouin-Jha, E. M. Parmentier, D. W. Sparks, *J. Geophys. Res.* **102**, 11979 (1997).
34. V. Maupin, *Geophys. J. R. Astron. Soc.* **83**, 379 (1985).
35. I calculated this temperature anomaly by comparing my 10- to 15-Ma model with a 4- to 20-Ma Pacific model (*20*). Between 50 and 150 km depth, the Reykjanes model is 70 m/s slower than the Pacific. Correcting this for the slowing effects of vertical fabric in the Reykjanes region reduces the velocity difference to 15 to 40 m/s. The temperature range is calculated assuming $\delta v_S/\delta T = -0.5\ \mathrm{m\ s^{-1}\ K^{-1}}$.
36. H. Jung, S.-I. Karato, *Eos (Fall Suppl.)* **81**, F1209 (2000).
37. G. Hirth, D. L. Kohlstedt, *Earth Planet. Sci. Lett.* **144**, 93 (1996).
38. J. W. Schlue, L. Knopoff, *Geophys. J. R. Astron. Soc.* **49**, 145 (1977).
39. Tabular and graphical representations of all five RR models are provided as supplemental data on *Science* Online (www.sciencemag.org/cgi/content/full/293/5535/1645/DC1).
40. Data were provided by Y. Shen and the IRIS Data Management Center (www.iris.washington.edu). I thank G. Hirth and D. Lizarralde for useful discussions. Supported by NSF grant EAR-9814565.

12 April 2001; accepted 18 July 2001

Climate Change as the Dominant Control on Glacial-Interglacial Variations in C_3 and C_4 Plant Abundance

Y. Huang,[1]* F. A. Street-Perrott,[2] S. E. Metcalfe,[3] M. Brenner,[4] M. Moreland,[5] K. H. Freeman[5]

Although C_4 plant expansions have been recognized in the late Miocene, identification of the underlying causes is complicated by the uncertainties associated with estimates of ancient precipitation, temperature, and partial pressure of atmospheric carbon dioxide ($P\mathrm{CO}_2$). Here we report the carbon isotopic compositions of leaf wax *n*-alkanes in lake sediment cores from two sites in Mesoamerica that have experienced contrasting moisture variations since the last glacial maximum. Opposite isotopic trends obtained from these two sites indicate that regional climate exerts a strong control on the relative abundance of C_3 and C_4 plants and that in the absence of favorable moisture and temperature conditions, low $P\mathrm{CO}_2$ alone is insufficient to drive an expansion of C_4 plants.

Plants use two principal carbon fixation pathways, the C_3 and C_4 cycles, during photosynthesis (*1*). C_4 plants (notably tropical grasses) are disadvantaged relative to C_3 plants (such as trees, shrubs, and cool-climate grasses) at high CO_2/O_2 ratios because of the additional energy expense needed to concentrate CO_2 in the bundle-sheath cells. At low CO_2/O_2, however, C_4 plants can achieve a relatively high quantum yield by suppressing photorespiration. The evolution of C_4 photosynthesis reflects an adaptation to the declining CO_2/O_2 ratio in Earth history (*2*). Based on this principle, expansions of C_4 plants in the late Miocene (*3*), Cretaceous (*4*), and last glacial maximum (LGM) (*5*, *6*) have been attributed

---

[1] Department of Geological Sciences, Brown University, Providence, RI 02912, USA. [2] Department of Geography, University of Wales Swansea, Swansea, SA2 8PP, UK. [3] Department of Geography, University of Edinburgh, Edinburgh, EH8 9XP, UK. [4] Department of Geological Sciences, University of Florida, Gainesville, FL 32611, USA. [5] Department of Geosciences, Pennsylvania State University, State College, PA 16802, USA.

*To whom correspondence should be addressed.

to decreases in atmospheric $P\mathrm{CO}_2$. The crossover between C_4 and C_3 photosynthesis occurs at lower growing season temperatures when $P\mathrm{CO}_2$ is reduced (*2*, *3*). However, studies of modern plant distributions indicate that precipitation also strongly affects the competitiveness of C_3 and C_4 plants. For example, the higher water-use efficiency of C_4 plants enables them to outcompete C_3 plants in hot dry environments with warm-season precipitation (*7*). Recent data (*8*) provide no evidence of declining $P\mathrm{CO}_2$ in the late Miocene, 7 to 8 million years ago (Ma), when populations of C_4 plants greatly expanded around the globe (*3*). Therefore, major scientific questions remain. Is a decrease in atmospheric $P\mathrm{CO}_2$ alone sufficient to trigger an expansion of C_4 plants in natural ecosystems? And can climatic factors, such as increased rainfall, counteract an increase in C_4 distribution due to lower $P\mathrm{CO}_2$?

Here, we present the results of stable carbon isotopic analyses of total organic carbon (TOC) and individual C_{27}, C_{29}, and C_{31} *n*-alkanes in sediment cores from two Mesoamerican sites, Lakes Alta Babícora and Quexil (Fig. 1). These sedimentary *n*-alkanes originate from the leaf waxes of terrestrial higher plants (both C_3 and C_4) (*4*, *9*). Carbon isotopic values of leaf wax *n*-alkanes are more diagnostic than those of TOC, which in lake sediments contains material of both terrestrial and aquatic origin (*9*). This study was designed to test the relative impacts of climate (i.e., aridity and seasonal precipitation) and $P\mathrm{CO}_2$ on the abundance of C_3 and C_4 plants. Paleoclimate data and General Circulation Model simulations show that these two sites were out of phase with respect to moisture availability as climate changed from the last glacial stage (LGS) to the early Holocene (*10*–*13*) (Fig. 1). The paleoclimatic gradient between them provides an excellent opportunity to test the importance of $P\mathrm{CO}_2$ versus regional climate on the relative abundance of C_3 and C_4 plants.

The Alta Babícora basin (29°N, 108°W) has a mean annual precipitation of 500 mm (mostly in July and August) and an average summer temperature of 20°C. The modern vegetation comprises shrub grassland with a significant C_4 component (*14*) on lower slopes and a mixed forest of pine (*Pinus*), oak (*Quercus*), and juniper (*Juniperus*) at higher altitudes. Multiproxy data are available for a 5.50-m core (*11*), of which the top 250 cm, spanning the past 20,000 years, was used for this study (Fig. 2). In contrast, Lake Quexil (16°55′N, 89°49′W) has annual precipitation (mainly in June through December) of 1600 mm and an annual mean temperature of 25°C. The modern vegetation is lowland semi-evergreen rainforest. Pollen (Fig. 3) and geochemical data have been published for a composite 19.6-m-long sediment sequence (cores 80-1 and H) (*12*). We used the uppermost part, spanning the past ~36,000 years, for this study.

The Alta Babícora microfossil data (from freshwater diatoms, *Pediastrum*, and high *Pinus* pollen) indicate the presence of a deep lake (19 m) in the LGS (*11*), whose primary moisture source was the Pacific in winter (Fig. 1) (*10*, *11*, *13*). A higher lake level reflects increased precipitation minus evaporation (P – E), which enhanced the soil water available to plants. The δ^{13}C values of C_{27}, C_{29}, and C_{31} *n*-alkanes (*15*, *16*) parallel those of TOC (Fig. 2). Between 20,700 and 12,700 ^{14}C years before the present (yr B.P.) (measured in the core from 210 to 143 cm), $\delta^{13}C_{\mathrm{TOC}}$ ranged from –24 to –22 per mil (‰), whereas individual leaf wax *n*-alkanes (C_{27}, C_{29}, and C_{31} *n*-alkanes) ranged from –30 to –26‰. The mean $\delta^{13}C_{\mathrm{TOC}}$ value for C_3 plants is –27‰ (range –33 to –22‰), and for C_4 –is 13‰ (range, –16 to –9‰) (*3*). For individual leaf wax *n*-alkanes, δ^{13}C values are ~6 to 8‰ lower than for bulk tissues, giving average *n*-alkane values of –34‰ for C_3 plants and –19‰ for C_4 plants (*17*). Thus, the δ^{13}C values of both TOC and individual leaf waxes indicate a predominance of C_3 plants.

In the early Holocene, lake levels fell dramatically. *Pediastrum* declined and Chenopodiaceae (chenopods), probably growing on desiccated lake muds, became more abundant (*11*). Diatom valve preservation was poor, suggesting shallow, turbid, alkaline conditions. Maximum dryness occurred around 6000 ^{14}C yr B.P. (*18*). Between 12,700 and 10,000 ^{14}C yr B.P. (core measurement, 143 to 130 cm), the δ^{13}C values of C_{27} and C_{29} *n*-alkanes increased rapidly from about –30 to –24‰, indicating an expansion of C_4 plants. $\delta^{13}C_{\mathrm{TOC}}$ shows a smaller increase, probably reflecting a partly aquatic origin for the TOC (*9*). Increases in the δ^{13}C values of both leaf wax *n*-alkanes and TOC occurred in the early Holocene, ~10,000 ^{14}C yr B.P. The δ^{13}C values indicate that C_4 plants predominated around the lake during most of the Holocene.

The $\delta^{13}C_{\mathrm{TOC}}$ profile from Lake Quexil differs from those of individual leaf waxes (Fig. 3), suggesting that the TOC comprises material from both terrestrial and aquatic sources. This is confirmed by the presence in the lipid fraction of abundant hopanoids with low δ^{13}C values (–70 to –50‰), derived from methanotrophic bacteria, as well as algal sterols. Therefore, only the δ^{13}C values of individual leaf wax *n*-alkanes are used here to infer changes in the proportion of C_3 and C_4 plants. The base of the sequence (>27,000 ^{14}C yr B.P.) is characterized by relatively low leaf wax δ^{13}C values (–34 to –31‰), suggesting a large C_3 component. Pollen data record a high abundance of *Pinus*, *Quercus*, and temperate trees, and a relatively low occurrence of Chenopodiaceae (Fig. 3) (*12*). δ^{13}C values increased to a maximum (–28 to –27‰) around the LGM (18,000 ^{14}C yr B.P.), implying enhanced C_4 plant input. The δ^{13}C maximum coincides with gypsum deposition and high charcoal concentrations (Fig. 3), indicating strongly evaporative conditions with frequent fires. Although lower humidity may cause a small increase in the δ^{13}C values of some C_3 species (*19*), the isotopic shift is too large to be interpreted merely as a humidity effect on C_3 plants. Using a binary model with endpoints of –19‰ for C_4 plant wax and –34‰ for C_3 plant wax (*16*), the relative contribution from C_4 plants at the LGM was about 40%. Substantial changes also occurred in the pollen assemblages: *Pinus* and *Quercus* declined considerably, whereas Chenopodiaceae and herbs (many of them C_4 plants) increased in abundance, which is consistent with the changes in leaf wax δ^{13}C values.

A 6 to 8‰ decrease in δ^{13}C values during

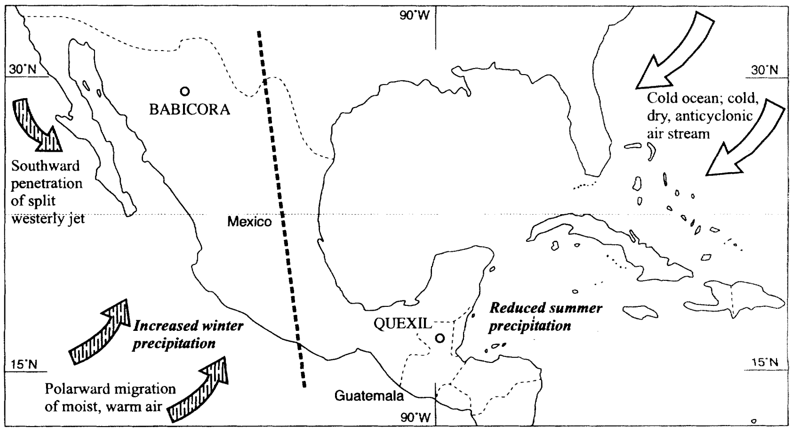

Fig. 1. Location of Lakes Alta Babícora and Quexil, showing moisture conditions in Mesoamerica during glacial times (27,000 to 13,000 years ago) and possible moisture sources (arrows) (*13*). The heavy dashed line separates sites that were effectively wetter than today (left) because of increased winter precipitation and those that were drier (right).

the early Holocene (10,000 to 8000 ^{14}C yr B.P.) reflects a shift to an overwhelming predominance of C_3 plants around Lake Quexil. Tropical trees, Melastomataceae, and *Quercus* become abundant in the pollen diagram (Fig. 3). However, carbon isotopic values of leaf wax *n*-alkanes increased by up to 5‰ in the mid- and late Holocene, corresponding to a palynologically documented decline in trees and an increase in herbs. This shift is attributable to anthropogenic forest clearance (*12*), exacerbated by regional drying (*20*), both of which would have favored C_4 grasses (*1*, *7*). Surface sediments from Quexil yield low $\delta^{13}C$ values (–35 to –34‰) for individual leaf waxes, consistent with the dominance of C_3 plants in the modern vegetation as a result of forest recovery after the collapse of the Mayan civilization.

In Fig. 4, the $\delta^{13}C$ values of the C_{29} *n*-alkanes from the Lake Babícora and Quexil cores are plotted versus age for the past 27,000 calendar (cal.) yr B.P., together with the ambient CO_2 concentration from the Taylor Dome ice core, Antarctica. The two sites show generally opposing temporal trends in the relative abundance of C_3 and C_4 plants. The isotopic data from Alta Babícora indicate a much greater abundance of C_3 plants during the LGM than during the Holocene. Lower

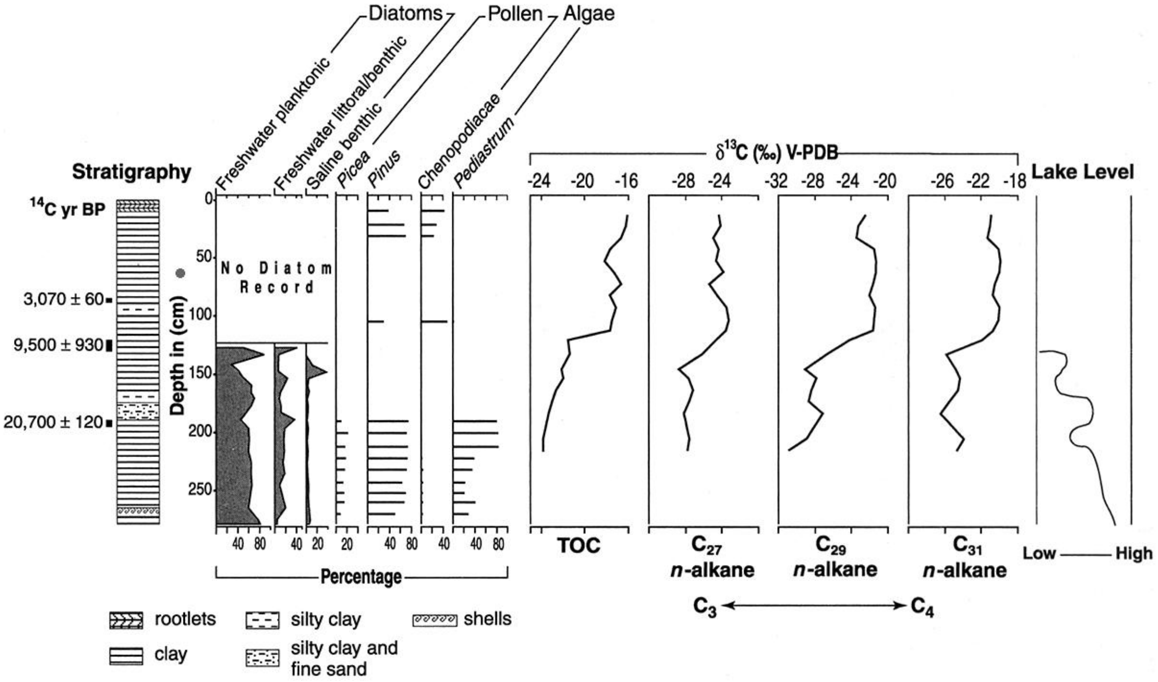

Fig. 2. Stratigraphy of bulk sediment properties, pollen and diatom assemblages, and carbon isotope values in core AB/94-3, Lake Alta Babícora, Mexico, with inferred lake level changes (*11*). $\delta^{13}C$ values of both TOC and individual leaf wax *n*-alkanes (C_{27}, C_{29}, and C_{31} *n*-alkanes) are shown.

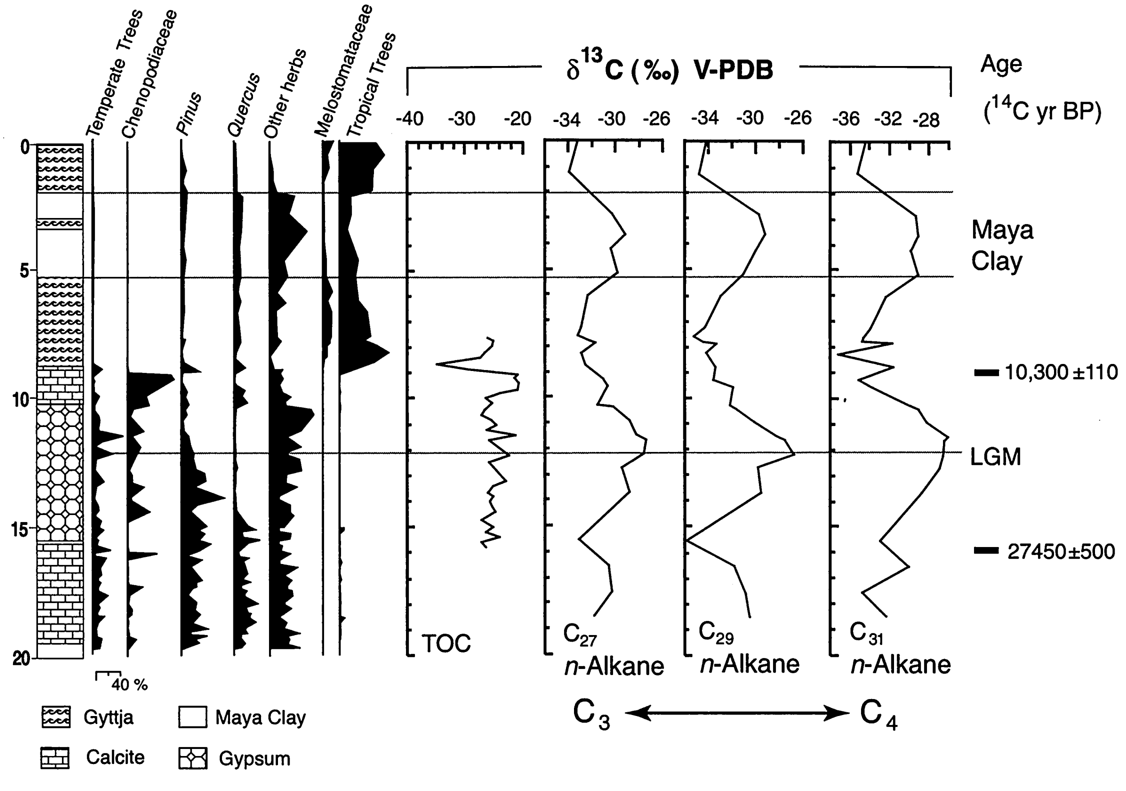

Fig. 3. Stratigraphy of bulk sediment properties, pollen assemblages (the pollen category "other herbs" includes grasses, composites, and sedges), and carbon isotope values of TOC and individual leaf waxes (C_{27}, C_{29}, and C_{31} *n*-alkanes) in cores 80-1 (depth, 19.6 to 8.8 m) and H (depth, 8.8 to 0 m) from Lake Quexil, Guatemala. The horizon of the LGM is based on linear interpolation between accepted ^{14}C dates (i.e., 10,700 ± 110 and 27,450 ± 500 ^{14}C yr B.P.). The lower and upper boundaries of the Maya Clay are dated 1700 and 400 cal. yr B.P., respectively (*12*).

atmospheric $P\mathrm{CO}_2$, which favors C_4 plants, was apparently offset by enhanced winter rainfall and lower temperatures, which would have favored C_3 plants (*1*). In contrast, during the Holocene, the combination of drier conditions, with summer moisture coming from the Gulf of Mexico, and higher temperatures would have favored C_4 plants. Thus, data from Alta Babícora demonstrate that regional climate exerted a greater control over the relative abundances of C_3 and C_4 plants than did $P\mathrm{CO}_2$.

Vegetation change at Quexil was also the net effect of several competing factors. At the LGM, the combined effects of low $P\mathrm{CO}_2$, aridity, and increased fire frequency apparently overwhelmed the effect of lower temperatures, leading to a higher relative abundance of C_4 plants. In the early Holocene, higher $P\mathrm{CO}_2$ and wetter climate offset the impact of rising temperatures, leading to the dominance of C_3 tropical trees. Anthropogenic land clearance, perhaps combined with regional drying, accounts for the increase in C_4 plants during the deposition of the "Maya Clay" about 1700 to 400 cal. yr B.P. (*12*). Surface sediments show a return to C_3 dominance, reflecting the modern semideciduous forest.

Our results indicate that the relative abundance of C_4 versus C_3 plants is controlled by complex interactions between several environmental factors, including rainfall, precipitation seasonality, temperature, and $P\mathrm{CO}_2$. The Alta Babícora record shows that even at the minimum atmospheric $P\mathrm{CO}_2$ during the LGM, the combined effect of high winter precipitation and low temperatures led to an expansion of C_3 plants. Greater C_4 plant abundance only occurred when low $P\mathrm{CO}_2$ coincided with increased aridity, as observed during the LGM at Quexil, and in tropical Africa and India (*5*, *9*, *16*, *21*, *22*). Studies of modern C_4 plant distributions confirm the importance of regional climatic controls. C_4 photosynthesis is commonly associated with hot dry environments with warm-season precipitation and high light intensities, because C_4 plants exhibit greater efficiency than C_3 species with respect to water, light, and nitrogen use (*1*, *7*). We conclude that in the absence of favorable climatic conditions, low $P\mathrm{CO}_2$ alone is insufficient to trigger the expansion of C_4 plants. Various lines of evidence support the importance of climate control on the relative abundance of C_3 and C_4 plants. Carbon isotopic data on organic matter from paleosols in the western U.S. Great Plains suggest increased C_3 plant abundance during the LGS (*23*, *24*), countering the $P\mathrm{CO}_2$ variation. Those authors suggest that lower temperatures, rather than lower atmospheric $P\mathrm{CO}_2$, were the main control on the relative abundance of C_3 and C_4 plants in this region. Late Miocene and Pliocene expansions of C_4 plants occurred at different rates and times between 8 and 3 Ma in different parts of the world (*25*, *26*). These geographic differences in the timing of C_4 plant proliferation indicate the importance of regional climate as opposed to atmospheric $P\mathrm{CO}_2$ control, which would otherwise have led to a globally synchronous C_4 plant expansion. Estimates of Miocene atmospheric $P\mathrm{CO}_2$ based on the alkenone paleobarometer (*8*) provide no evidence for decreased $P\mathrm{CO}_2$ in the late Miocene. Those authors suggest that the late Miocene radiation of C_4 plants around the globe resulted from increasing seasonality and aridity rather than an abrupt decline in $P\mathrm{CO}_2$, a conclusion supported by faunal and floral changes (*27*), rising $\delta^{18}O$ values of paleosol carbonate (*25*), enhanced dust fluxes in the Pacific (*28*), and deeper soil calcic horizons (*29*).

Although we accept that C_4 photosynthesis evolved primarily in response to the long-term decline in atmospheric $P\mathrm{CO}_2$ over the past 100 million years (*1*), we conclude that $P\mathrm{CO}_2$ levels during the past 15 million years were sufficiently low to create conditions that generally, but not decisively, favored C_4 plants. Large-scale expansions of C_4 plants were triggered primarily by major changes in precipitation and temperature in low-latitude regions. However, accurate predictions of future vegetation changes must take into account all three key factors, including $P\mathrm{CO}_2$ alongside predicted changes in temperature and precipitation patterns.

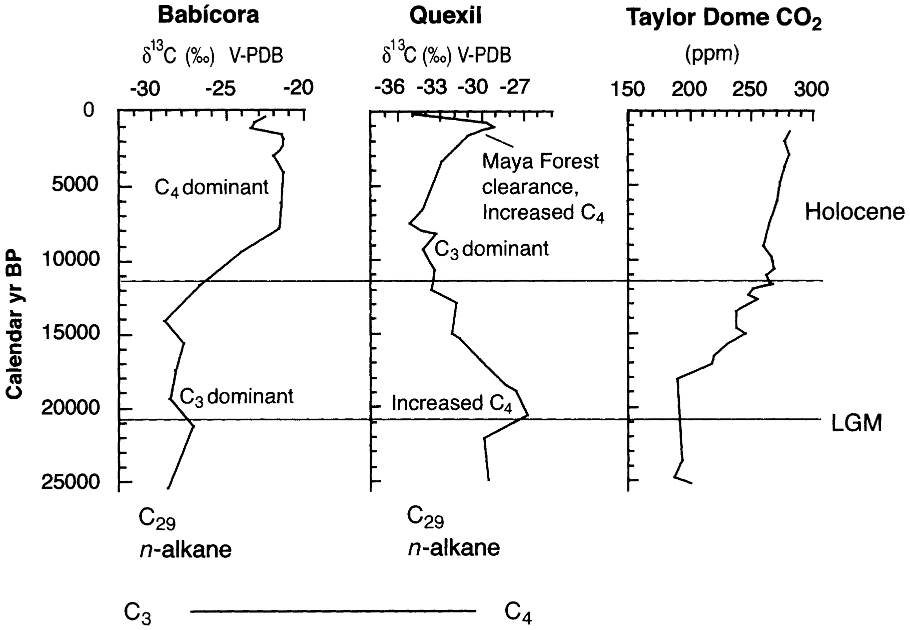

Fig. 4. Variations in $\delta^{13}C$ values of C_{29} *n*-alkanes from Lakes Alta Babícora and Quexil, compared with atmospheric CO_2 variations during the past 27,000 calendar years as recorded by the Taylor Dome ice core, Antarctica (*30*).

References and Notes

1. R. F. Sage, in *C_4 Plant Biology*, R. F. Sage, R. K. Monson, Eds. (Academic Press, San Diego, CA, 1999), pp. 3–16.
2. J. R. Ehleringer, T. E. Cerling, B. R. Helliker, *Oecologia* **112**, 285 (1997).
3. T. E. Cerling *et al.*, *Nature* **389**, 153 (1997).
4. M. M. M. Kuypers, R. D. Pancost, J. S. Sinningghe Damsté, *Nature* **399**, 342 (1999).
5. F. A. Street-Perrott *et al.*, *Science* **278**, 1422 (1997).
6. D. R. Cole, H. C. Monger, *Nature* **368**, 533 (1994).
7. E. D. Schulze, R. Ellis, W. Schulze, P. Trimborn, *Oecologia* **106**, 352 (1996).
8. M. Pagani, K. H. Freeman, M. A. Arthur, *Science* **285**, 876 (1999).
9. Y. Huang, F. A. Street-Perrott, R. A. Perrot, P. Metzger, G. Eglinton, *Geochim. Cosmochim. Acta* **63**, 1383 (1999).
10. COHMAP Members, *Science* **241**, 1043 (1988).
11. S. E. Metcalfe, A. Bimpson, A. J. Courtice, S. L. O'Hara, D. M. Taylor, *J. Paleolimnol.* **17**, 155 (1997).
12. B. W. Leyden, M. Brenner, D. A. Hodell, J. H. Curtis, *Palaeogeogr. Palaeoclimatol. Palaeoecol.* **109**, 193 (1994).
13. J. P. Bradbury, *Quat. Int.* **43/44**, 97 (1997).
14. S. L. Connin, J. Betancourt, J. Quade, *Quat. Res.* **50**, 179 (1998).
15. Sediment samples were freeze-dried and extracted three times ultrasonically with 2:1 methylene chloride/methanol. Total lipid extracts were separated into different classes by silica gel flash-column chromatography. Elution with hexane gave aliphatic hydrocarbon fractions, which contain long-chain (C_{25} to C_{31}) *n*-alkanes with strong odd-over-even carbon predominance. Urea adduction and thin-layer chromatography using plates containing 5% $AgNO_3$ were used to obtain clean *n*-alkanes for complex samples. The carbon preference index (*9*) for *n*-alkanes ranges from 3.6 to 10 in Quexil sediments and from 4 to 7 in Alta Babícora sediments. Carbon isotopic compositions of leaf wax *n*-alkanes were measured by gas chromatography (GC)–combustion–isotope ratio mass spectrometry (IRMS) at either Brown University or Pennsylvania State University [see (*16*) for a description of the method]. At Brown, an HP6890 GC is connected to a Finnigan MAT Delta^{+}-XL mass spectrometer via a GC-C III interface. Organic compounds were oxidized into CO_2 for $\delta^{13}C$ measurements at 940°C when flowing through a ceramic oxidation reactor bearing three braided NiO/CuO/Pt wires. Six pulses of standard CO_2 gases, precalibrated against a commercial reference CO_2 [ZTECH, Dallas, TX; −10.07‰ versus the Pee Dee

belemnite (PDB) standard], were injected via the GC-C III interface to the IRMS for the computation of $\delta^{13}C$ values of sample compounds. A set of standard *n*-alkanes with known $\delta^{13}C$ values acquired from Indiana University were measured before sample analyses to ensure accuracy of the $\delta^{13}C$ measurement. The standard deviation for duplicate analyses is $< \pm 0.3‰$. $\delta^{13}C$ TOC was determined by combusting decarbonated (with 10% HCl) sediments in an elemental analyzer and subsequently collecting and cryogenically purifying the evolved CO_2. The CO_2 samples were then measured on dual-inlet IRMS for isotopic ratios. For Alta Babícora sediments, a cold finger was used to further concentrate the CO_2 for measurement because of the exceptionally low organic content (0.2 to 0.6%). Carbon isotope values are expressed relative to the V-PDB standard.

16. Y. Huang, K. H. Freeman, T. I. Eglinton, F. A. Street-Perrott, *Geology* **27**, 471 (1999).
17. G. Rieley, J. W. Collister, B. Stern, G. Eglinton, *Rapid Commun. Mass Spectrom.* **7**, 488 (1993).
18. J. Ortega Ramírez, *Geofis. Int.* **34**, 107 (1995).
19. D. G. Williams, J. R. Ehleringer, *Oecologia* **106**, 455 (1996).
20. D. A. Hodell, J. H. Curtis, M. Brenner, *Nature* **375**, 391 (1995).
21. M. R. Talbot, T. Johannesson, *Earth Planet. Sci. Lett.* **110**, 23 (1992).
22. R. Sukumar, R. Ramesh, R. K. Pant, G. Rajagopalan, *Nature* **364**, 703 (1993).
23. T. W. Boutton, S. R. Archer, L. C. Nordt, *Nature* **372**, 625 (1994).
24. D. R. Muhs *et al.*, *Geol. Soc. Am. Bull.* **111**, 1861 (1999).
25. C. Latorre, J. Quade, W. C. McIntosh, *Earth Planet. Sci. Lett.* **146**, 83 (1997).
26. M. E. Morgan, J. D. Kingston, B. D. Marino, *Nature* **367**, 162 (1994).
27. R. L. Bernor *et al.*, in *The Evolution of Western Eurasian Neogene Mammal Faunas*, R. L. Bernor, V. Fahlbusch, H. W. Mittmann, Eds. (Columbia Univ. Press, New York, 1996), p. 449.
28. D. K. Rea, H. Snoeckx, L. H. Joseph, *Paleoceanography* **13**, 215 (1998).
29. G. J. Retallack, *Palaios* **12**, 380 (1997).
30. H. Fischer, personal communication.

31. We thank T. Webb III and S. C. Clemens for insightful comments, M. F. Rosenmeier and J. H. Curtis for kind assistance during subsampling of Quexil sediment cores, B. W. Leyden for supplying Quexil pollen data, H. Fischer for supplying CO_2 data from the Taylor Dome ice core, and B D. Walizer for assistance during $\delta^{13}C$ TOC analyses. Supported by grants from NSF (EAR-9814584 and ATM-0081478) and the American Chemical Society–Petroleum Research Fund (35208-G2).

23 February 2001; accepted 31 July 2001

Regulation of Transcriptional Activation Domain Function by Ubiquitin

Simone E. Salghetti,[1] Amy A. Caudy,[1,2] Joshua G. Chenoweth,[3] William P. Tansey[1]*

The ability of transcriptional activation domains (TADs) to signal ubiquitin-mediated proteolysis suggests an involvement of the ubiquitin-proteasome pathway in transcription. To probe this involvement, we asked how ubiquitylation regulates the activity of a transcription factor containing the VP16 TAD. We show that the VP16 TAD signals ubiquitylation through the Met30 ubiquitin-ligase and that Met30 is also required for the VP16 TAD to activate transcription. The requirement for Met30 in transcription is circumvented by fusion of ubiquitin to the VP16 activator, demonstrating that activator ubiquitylation is essential for transcriptional activation. We propose that ubiquitylation regulates TAD function by serving as a dual signal for activation and activator destruction.

Many transcription factors are unstable proteins that are destroyed by ubiquitin (Ub)-mediated proteolysis (*1*), a process in which covalent attachment of Ub to proteins signals their destruction by the proteasome (*2*). In most transcription factors, the domain that signals their ubiquitylation—the "degron"—overlaps closely with a transcriptional activation domain (TAD). Indeed, this overlap is both widespread and intimate: Mutational analysis of TADs (*3*–*5*) reveals a close correlation between transcriptional activation and proteolysis. The unexpected convergence of transcription and proteolytic signaling elements raises the possibility that the Ub-proteasome pathway is involved in transcription. We tested this hypothesis by examining the role that the ubiquitylation machinery plays in transcriptional activation by the VP16 activation domain (*6*).

Substrate targeting by the ubiquitylation machinery is carried out by Ub-ligases (*2*), which interact with the degron and recruit Ub-conjugating enzymes to the substrate protein. Because of the key role of Ub-ligases in substrate recognition, we sought to identify the Ub-ligase that targets the VP16 TAD in *Saccharomyces cerevisiae*. We fused the VP16 TAD to the bacterial DNA binding protein LexA (*7*) and expressed the fusion protein in yeast. For comparison, we also fused LexA to the TAD-degrons from Myc (*3*) and from the yeast cyclin Cln3 (*5*). Pulse-chase analysis (Fig. 1A, lanes 1 through 4) revealed that all three TADs acted as degrons in this setting, destabilizing the LexA protein. To identify the Ub-ligase for VP16, we next examined the stability of LexA-VP16 in yeast strains defective for various components of the Ub-proteasome pathway, including Ubc2, Cdc4, Met30, and Grr1. This analysis revealed that LexA-VP16 was stabilized by loss of Met30 (Fig. 1A), a substrate-recognition component of the SCF Ub-ligase family (*8*). The dependence on Met30 was specific to LexA-VP16 because deletion of *Met30* had little effect on the stabilities of LexA-Myc and LexA-Cln3 (Fig. 1A). Consistent with a specific role for Met30 in VP16 degron function, Met30 associated with LexA-VP16—and not other LexA-fusion proteins—in vitro (Fig. 1B, compare lanes 2 and 4 with lane 6), and Met30 was required for LexA-VP16 ubiquitylation in vivo (Fig. 1C, compare lanes 3 and 6) (*9*). Taken together, these data demonstrate that the Met30 Ub-ligase is specifically required for degron function of the VP16 TAD.

We next examined whether loss of Met30 affected transcriptional activation by VP16 (Fig. 2). A modified GAL1 promoter carrying two LexA binding sites and driving expression of β-galactosidase (*10*), was integrated into yeast strains that either contained or lacked a functional *Met30* locus. We then measured the ability of each LexA fusion protein to activate reporter gene expression in these cells (Fig. 2A, transcription). As expected, the Myc, Cln3, and VP16 TADs potently activated reporter gene expression in the presence of Met30. However, in the absence of Met30, the VP16 TAD failed to activate β-galactosidase expression. As observed with proteolysis (Fig. 1A), the effect of loss of Met30 was specific to VP16 because transcriptional activation by LexA-Myc and LexA-Cln3 remained constant. Thus, although the LexA-VP16 activator is more stable and accumulates to twofold higher levels (Fig. 2A, protein) in *Met30*-null cells, it is unable to activate transcription in the absence of Met30 (*11*). The specific loss of VP16 transcriptional activity reveals that Met30 plays an essential role in both the TAD and degron function of the VP16 activation domain.

To determine whether loss of Met30 attenuates VP16 activity through an indirect mechanism, we asked whether LexA-VP16 displays any activity in *Met30*-null cells. Chromatin immunoprecipitation (ChIP) analysis (Fig. 2B) revealed that LexA-VP16 efficiently interacts with promoter DNA in the absence of Met30 in vivo (compare lanes 3 and 6), demonstrating that there is not a global defect in the folding or

---

[1] Cold Spring Harbor Laboratory, 1 Bungtown Road, Post Office Box 100, Cold Spring Harbor, NY 11724, USA. [2] Watson School of Biological Sciences, Cold Spring Harbor Laboratory, Cold Spring Harbor, NY 11724, USA. [3] Graduate Program in Molecular and Cellular Biology, State University of New York at Stony Brook, Stony Brook, NY 11794, USA.

*To whom correspondence should be addressed. E-mail: tansey@cshl.org